Int. J. Nano Dimens., 11 (3): 222-236, Summer 2020

ORIGINAL ARTICLE

Design of a new asymmetric waveguide in InP-Based multi-quantum well laser

Zahra Danesh Kaftroudi [1*], *Abolfazl Mazandarani* [2]

[1] *Department of Engineering Sciences, Faculty of Technology and Engineering East of Guilan, University of Guilan, 44891-63157, Rudsar-Vajargah, Iran.*
[2] *Plasma & Nuclear Fusion Research School, Nuclear Science & Technology Research Institute, Tehran, Iran.*

Received 12 November 2019; revised 11 May 2020; accepted 14 May 2020; available online 25 May 2020

Abstract

Today, electron leakage in InP-based separate confinement laser diode has a serious effect on device performance. Control of electron leakage current is the aim of many studies in semiconductor laser industry. In this study, for the first time, a new asymmetric waveguide structure with n-interlayer for a 1.325 μm InP-based laser diode with InGaAsP multi-quantum well is proposed and theoretically analyzed using the PICS3D simulation software. The simulator self-consistently combines the 3D simulation of carrier transport, self-heating, and optical waveguiding. Through the simulation, the optical and electrical performances of laser diodes with symmetric and asymmetric waveguides are studied. Numerical simulation reveals that the asymmetric structure exhibits higher output light power, slope efficiency, emission intensity, and series resistance, as well as lower electron leakage and threshold current density under identical conditions, compared with the symmetric structure. The performances are greatly enhanced in the laser diode with asymmetric waveguide design because of the improved radiative stimulated recombination rate, declined non-radiative Auger recombination rate and decreased overlap between the optical wave and the p-doped layer.

Keywords: *Asymmetric Waveguide; Electron Leakage; InGaAsP; Optimization; PICS3D; Quantum Well; Simulation.*

How to cite this article

Danesh Kaftroudi Z., Mazandarani A. Design of a new asymmetric waveguide in InP-Based multi-quantum well laser. Int. J. Nano Dimens., 2020; 11 (3): 222-236.

INTRODUCTION

Electrically-injected diode lasers have been reported in many compound semiconductor material systems, including GaAs, InP, GaSb, and GaN for obtaining coherent light emitters with frequencies ranging from ultraviolet to mid-infrared. Consequently, high-power and high-efficiency diode lasers have been widely utilized in different applications including communications, imaging, remote sensing, displays, manufacturing, and healthcare [1, 2].

In a modern semiconductor laser designing, InGaAsP/InP is one of the practical material systems. Long-wavelengths (up to 1μm) are needed as optical sources for telecommunications. The most serious problem in a device with an InGaAsP active region is electron leakage due to small conduction band offset, which leads to high mobility of electron escaping from the multi-quantum well. There are many examples in the literature about the reduction of electron leakage by optimizing the structure of laser diodes. Among them, strained-layer multi-quantum barrier (MQB) has been widely employed [3-6]. This proposal is used to prevent electron escaping into the p-cladding layer by increasing the effective barrier's height in the p-type regions.

* Corresponding Author Email: Zahraadaneh@guilan.ac.ir

Advanced semiconductor laser design approaches employ various waveguide designs for improving the characteristics of laser diodes. One way to optimize laser performance by engineering the waveguide design is to use an asymmetric waveguide design. Numerous studies have been conducted on asymmetric waveguide laser diodes. The suggested structures include the use of a separate "optical trap layer on the n-side of the active region, doping the n-type waveguide layer with p-type doping, and asymmetric broad waveguide [7-9].

Today, simulation is very important in industry. Simulation decreases the cost, provides a fast information analysis, and saves time. It also leads to reaching a system with different configurations [10].

A conventional method for constructing an asymmetric waveguide is using p-separate confinement heterostructure layer and n-separate confinement heterostructure layer with different thicknesses and different cladding compositions [11, 12]. A more effective technique is the bandgap engineering. In this new method, an interlayer is employed in the p or n side of the laser cavity, which is introduced as interlayer [3, 12]. To our knowledge, few studies exist on the asymmetric waveguide structure for InGaAsP multi-quantum well lasers [12, 13]. Comparison of the experimental results that reported by Qing for 1.55 **μm** InGaAsP confirms that the interlayer method improves laser performance more effectively than the conventional method [12, 13]. Qing [12] used p-interlayer in the InGaAsP laser structure. For this structure, the threshold current and the maximum output power were reported 41mA and 180 mW, respectively. But for the conventional asymmetric waveguide LD, the threshold current was 276 mA and the maximum output power was 160 mW [13]. Here, for the first time, we propose and analyze theoretically a new asymmetric waveguide structure for 1.325 **μm** InP-based laser diode with InGaAsP multi- quantum well. The novelty of our design is based on employing the n-interlayer for achieving optimal performance using the PICS3D simulation software. The simulator self-consistently combines the 3D simulation of carrier transport, self-heating, and optical waveguiding. Through the simulation, the optical and electrical performances of laser diodes with symmetric and asymmetric waveguides are studied (for the purpose of simplicity, they will be called structure B and structure A, respectively). The simulation results indicate that after using asymmetric waveguide structure, the electron leakage is reduced, leading to the improved characteristics of laser diodes, including threshold current and output power.

The remainder of this paper is organized as follows: In Section 2, the device structure and theoretical models are introduced. The simulation results are discussed and presented in Section 3. Finally, in Section 4, some concluding remarks are presented.

MATERIALS AND METHODS

The simulation example in this article is a typical InGaAsP multi-quantum well (MQW) laser diode grown on InP. The MQW active region consists of six 0.006 μm thick 1.2% compressively strained InGaAsP quantum wells. The large compressive strain is preferred in order to reduce the threshold and increase the gain coefficient. The 0.01μm thick barriers exhibit no strain. For the given wells, the barrier thickness is selected as 0.01 μm thick to avoid any bounded state coupling among the different wells. In structure B, Fig. 1(a), the MQW stack is sandwiched between a pair of un-doped 0.17 μm thick lattice matched InGaAsP separate confinement layers (SCLs), which acts as a symmetric waveguide (common design). Above and below the waveguide in the structure, heavily doped p- and n-type (2×10^{18} cm^{-3}) InP cladding layers are used to improve the electrical current injection. A highly doped p-InP contact layer is employed to complete the entire laser structure. In structure A, Fig. 1(b), an un-doped 0.17 μm thick lattice matched InGaAsP interlayer between the n-SCL and n-cladding layers is introduced with the other parts of the laser structure left unchanged. The Fabry-Perot resonator lengths are considered to be 500 μm. Both of the laser's facets are given a reflectivity of 32%. Fig. 1 shows the symmetric and the asymmetric waveguide lasers.

The composition, doping level, and thickness of the layers in both laser structures (B , A) are given in Table 1 and Table 2, respectively.

Considering the technological importance of semiconductor lasers, it is crucial to be able to perform a predictive simulation of new device designs before actual manufacturing of devices. Simulation leads to optimization of the laser structures. In this work, the laser simulation is performed using the PICS3D (Photonic Integrated

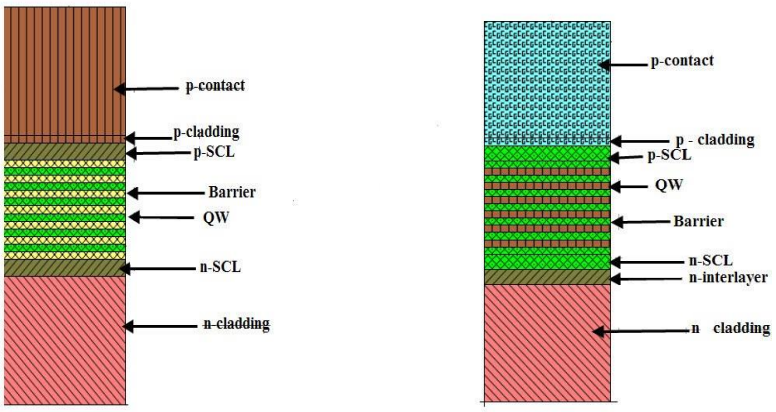

(a) (b)

Fig. 1. Schematic diagrams of (a) symmetric waveguide laser diode (structure B) (b) asymmetric waveguide laser diode (structure A).

Table 1. The epitaxial symmetric layer structure.

Layer	Doping (cm^{-3})	Thickness (μm)
n-InP (substrate)	2×10^{18}	40
InP (n-cladding)	2×10^{18}	1.3
i-$In_{0.87}Ga_{0.13}As_{0.28}P_{0.72}$(n-SCL)	Un-doped	0.17
i-$In_{0.87}Ga_{0.13}As_{0.28}P_{0.72}$(Barrie×7)	Un-doped	0.01
i-$In_{0.936}Ga_{0.064}As_{0.51}P_{0.49}$(QW×6)	Un-doped	0.006
i-$In_{0.87}Ga_{0.13}As_{0.28}P_{0.72}$(p-SCL)	Un-doped	0.17
InP (p-cladding)	2×10^{18}	0.02
p-InP (contact)	2×10^{18}	1.3

Table 2. The epitaxial symmetric layer structure.

Layer	Doping (cm^{-3})	Thickness (μm)
n-InP (substrate)	2×10^{18}	40
InP (n-cladding)	2×10^{18}	1.3
i-$In_{0.932}Ga_{0.068}As_{0.15}P_{0.75}$(n-interlayer)	Un-doped	0.17
i-$In_{0.87}Ga_{0.13}As_{0.28}P_{0.72}$(n-SCL)	Un-doped	0.17
i-$In_{0.87}Ga_{0.13}As_{0.28}P_{0.72}$(Barrie×7)	Un-doped	0.01
i-$In_{0.936}Ga_{0.064}As_{0.51}P_{0.49}$(QW×6)	Un-doped	0.006
i-$In_{0.87}Ga_{0.13}As_{0.28}P_{0.72}$(p-SCL)	Un-doped	0.17
InP (p-cladding)	2×10^{18}	0.02
p-InP (contact)	2×10^{18}	1.3

Circuit Simulator in 3D) software package. It provides a 3D analysis based on the Finite Element (FE) method by coupling the multiple 2D cross-sections of a waveguide device with a round-trip gain equation (Transfer Matrix Method) for propagation. In the longitudinal direction, Effective Index Method (EIM) is usually used for finding lateral optical modes. Equations for electrical, optical, and thermal phenomena are coupled together and solved self-consistently to give an accurate description of device characteristics. Advanced quantum well models such as those for k.p theory or many-body effects are implemented [14].

The electrical behavior of an InP-based semiconductor device is described with the FE drift-diffusion model in this package [15]:

$$-\nabla.\left(\frac{\varepsilon_0\varepsilon_{dc}}{q}\nabla V\right)=-n+p+N_D\left(1-f_D\right)- N_A+\sum_j N_t\left(\delta_j-f_{tj}\right). \quad (1)$$

$$\nabla.\mathbf{J_n} - \sum_j R_n^{tj} - R_{sp} - R_{st} - R_{Aug} + G_{opt}(t) = \frac{\partial n}{\partial t} + N_D \frac{\partial f_D}{\partial t}. \quad (2)$$

$$\nabla.\mathbf{J_p} + \sum_j R_p^{tj} + R_{sp} + R_{st} + R_{Aug} - G_{opt}(t) = -\frac{\partial p}{\partial t} + N_A \frac{\partial f_A}{\partial t}. \quad (3)$$

The model is primarily governed by three equations. One is Poisson's equation, expressed by Eq. (1). The others are current continuity equation for electrons and holes, shown by Eqs. (2) and (3), respectively. In Eq. (1), ε_0 and ε_{dc} represent the dielectric constant of vacuum and the relative dielectric constant, respectively. Also n and p are the electron and hole concentrations, respectively. N_D and N_A are the doping densities of shallow donors and shallow acceptors, respectively. N_{tj} is the density of the j_{th} deep trap, f_D and f_A are the occupancies of donor and acceptor levels, respectively, and f_{tj} is occupancy of the j_{th} deep trap level. In Eqs. (2) and (3), G_{opt} is the photon generation rate per unit volume, and R_{st}, R_{sp}, and R_{Aug} are the stimulated, spontaneous, and Auger recombination emission rates, respectively.

High-accuracy modeling of the optical and transport properties of semiconductors requires some information about the band structure. Dispersion of the valence band can be obtained by diagonalization of Luttinger_Kohn Hamiltonian in four-band approximation [15]:

$$\begin{pmatrix} P+Q & -S & R & 0 \\ -S^* & P-Q & 0 & R \\ R^* & 0 & P-Q & S \\ 0 & R^* & S^* & P+Q \end{pmatrix} \quad (4)$$

$$P = \frac{\hbar^2}{2m_0}\gamma_1(k_x^2+k_y^2+k_z^2) + P_\varepsilon + E_\upsilon(z),$$
$$Q = \frac{\hbar^2}{2m_0}\gamma_2(k_x^2+k_y^2-2k_z^2) + Q_\varepsilon,$$
$$S = \sqrt{3}\frac{\hbar^2}{m_0}\gamma_3 k_z(k_x - ik_y),$$
$$S = \sqrt{3}\frac{\hbar^2}{m_0}\gamma_3 k_z(k_x - ik_y),$$
$$R = \sqrt{3}\frac{\hbar^2}{2m_0}\gamma_2(k_x^2 - k_y^2 - 2\gamma_3 k_x k_y), \quad (5)$$
$$P_\varepsilon = -a_\upsilon(\varepsilon_{xx}+\varepsilon_{yy}+\varepsilon_{zz}),$$
$$Q_\varepsilon = -\frac{b}{2}(\varepsilon_{xx}+\varepsilon_{yy}-2\varepsilon_{zz}),$$
$$\varepsilon_{xx} = \frac{a_{st}-a_0}{a_0},$$
with $\varepsilon_{zz} = -2\frac{C_{12}}{C_{11}}\varepsilon_{xx}$,

where, ħ is the Planck's constant divided by 2π, m_0 is the free electron mass, k_x, k_y, and k_z are wave vector components, $E_v(z)$ is the confinement potential in the valence band, ε_{ij} represents strain tensor components, a_v and b are deformation potentials, C_{ij} stands for elastic constants, a_0 and a_{st} are the lattice constants for unstrained and strained structures, respectively, and $R^*$and $S^*$are the Hermitian conjugates of R_k and S_k, respectively, as generated by changing the sign in front of the imaginary unit *I*. The material constants γ_1, γ_2, and γ_3 are referred to as Luttinger parameters from the Hamiltonian matrix, the eigenvalues; and *E(k)* can be found by solving the determinantal equation [15]:

$$\det\left[H_{ij} - \delta_{ij}E\right] = 0. \quad (6)$$

The net optical gain *g* (hv) of stimulated carrier recombination (photon emission) and carrier generation (photon absorption) is a function of the photon energy *hv* [15]:

$$g(E) = \frac{g_0}{2\pi E t}\sum_{i,j}\int_0^\infty \frac{(\frac{\pi}{\Gamma})f_{dip}(k_t)M_b(f_j - f_i)d^2k_t}{1+\frac{(E_{cj}(k_t)-E_{kpi}-E)^2}{\Gamma^2}}. \quad (7)$$

where, *t* is the thickness of QW and $\Gamma = \hbar/\tau_{scat}$ is the broadening due to intraband scattering relaxation time τ_{scat}, E_{cj} is the j_{th} conduction subband, E_{kpi} is the i_{th} valence subband from the k.p calculation, the sum is over all possible conduction and valence subbands, $g_0 = \pi q^2\hbar/\varepsilon_0 cm^2 n_0$ is a constant with all symbols having their usual meanings, and M_b is a dipole moment [15]. The Fermi functions f_i and f_j give the probability that the energy levels E_{kpi} and E_{cj} are occupied by the electrons in the valence and conduction subbands, respectively and are defined as follows [15]:

$$f_{i,j}(E, E_{fn,fp}) = \frac{1}{1+\exp\left[\frac{E-E_{fn,fp}}{KT}\right]}. \quad (8)$$

$E_{fn,fp}$ represents the quasi-levels in the conduction and valence subbands, and k is Boltzmann constant. The electron and hole concentrations are defined by Fermi distribution and a parabolic density of state. For QWs, the following equations are given to express the density of electrons and holes in a QW [15]:

$$n = \sum_j \rho_j^0 \, KT \ln\left[1+e^{\left(\frac{E_{fn}-E_j}{KT}\right)}\right] + unconfined\ electrons. \quad (9)$$

$$p = \sum_i \rho_i^0 \, KT \ln\left[1+e^{\left(\frac{E_i-E_{fp}}{KT}\right)}\right] + unconfined\ holes. \quad (10)$$

where, the subscript i denotes all confined states for different hole bands, and j denotes those for the Γ band, and ρ is the parabolic density of states. The number of unconfined carriers is calculated using Fermi-Dirac statistics. These relations can be used as a recursive equation for calculating the quasi-Fermi levels, Fermi probability, and as consequently the QW laser gain spectrum.

For the treatment of device heating, the thermoelectric power and the thermal current induced by the temperature gradient are solved using the method provided by Wachutka [15]. Various heat sources, including Joule heat, generation/recombination heat, Thomson heat, and Peltier heat, are taken into account in this specific study. The software solves the scalar Helmholtz equation to obtain a transverse component of the optical field. The lateral components are given by the Bessel functions. Further details of the model can be found elsewhere [15].

There are three types of material in semiconductor laser simulation: semiconductors, insulators, and conductors. For each class, many material parameters exist that must be chosen before simulation. In our simulation, the material parameter of semiconductors is very important. For $In_{1-x}Ga_xAs_yP_{1-y}$ compounds which are used as active layer, SCL layers and interlayer layer, the linear interpolation formulas are used to compute the quaternary material parameters [15]:

$$T(In_{1-x}Ga_xAs_yP_{1-y}) = \quad (11)$$
$$\frac{\left[x(1-x)\left[yT_{InGaAs}(x)+(1-y)T_{InGaP}(x)\right]+y(1-y)\left[xT_{GaAsP}(y)+(1-x)T_{InAsP}(y)\right]\right]}{\left[x(1-x)+y(1-y)\right]}.$$

where x and y are the molar fractions and T is the ternary material parameter. Parameters of ternary alloys AB_xC_{1-x} are usually determined as [15]:

$$T(A_xB_{1-x}C) = xB(AC)+(1-x)B(BC). \quad (12)$$

where, x is the molar fraction and B is the binary material parameter. Table 3 presents the material parameters of the binary semiconductors such as InP, GaAs, InAs, and GaP used for calculating the $In_{1-x}Ga_xAs_yP_{1-y}$ material parameters. The $In_{1-x}Ga_xAs_yP_{1-y}$ composition dependence band gap (eV) is calculated by the following relationship [15]:

$$E_g\left(In_{1-x}Ga_xAs_yP_{1-y}\right) = 1.347-0.788y+0.149y^2 -$$
$$4.1\times10^{-4}\left[\frac{T^2}{T+136}\right]+8.4633030\times10^{-2}. \quad (13)$$

RESULTS AND DISCUSSIONS

Silica fiber optic is a major building block in the telecommunication infrastructure. Due

Table 3. Material parameters of the binary semiconductor in two systems used in this study.

Parameter	Unit	GaAs	InAs	GaP	InP
m_c	m_0	0.0665	0.027	0.13	0.064
γ_1	-	6.85	19.67	4.05	6.35
γ_2	-	2.1	8.37	0.42	2.08
γ_3	-	2.9	9.29	2.93	2.76
a_0	$\times10^{-4}$ μm	5.65325	6.058	5.4505	5.869
C_{11}	GPa	1181	8329	1405	1022
C_{12}	GPa	532	452.6	620.3	579
a_v	eV	1.16	1	1.7	0.6
b	eV	-2.0	-1.8	-1.6	-2.0

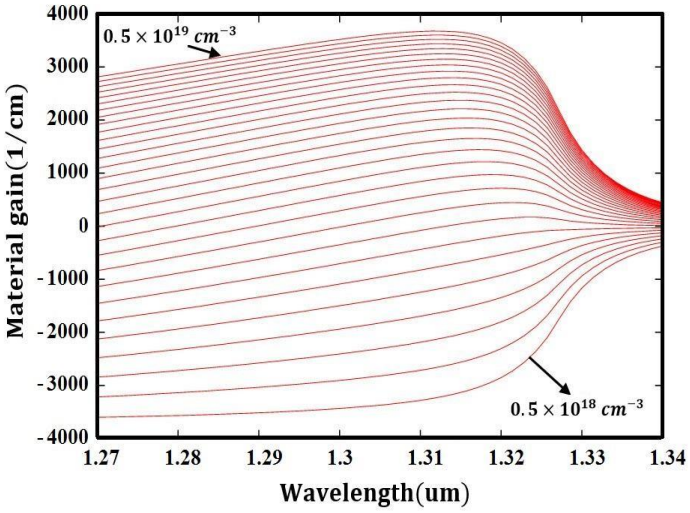

Fig. 2. Gain spectrum plotted at different carrier densities.

to its unique features, it can be ideal for gigabit transmission and a medium for carrying information in the form of light. An optical communication system consists of a transmitting device, an optical fiber cable and a receiver, each with its own functions. Silica fiber in optical communication uses wavelengths that are undetectable with unaided eye. Typical optical transmission wavelengths are 0.85, 1.3, and1.55µm. Good features of silica fiber at 1.3µm or 1.55 µm wavelengths have led to the rapid development of lasers operating at these wavelengths [16]. In this regard, the band gap of the material composing semiconductor lasers is required to correspond to the oscillation wavelengths of the laser diodes. The most successful laser diodes used in the mentioned wavelengths are based on the quaternary III-V semiconductor alloys. Typical compound semiconductors that meet these conditions are GaInAsP and AlGaInAs grown on the InP substrate [17]. The performance of the laser diodes has been dramatically improved by applying strained quantum well structures as their active region. Direct electron and hole recombination in InGaAsP MQW are the source of the photon emission. When the injected carrier densities (electrons and holes) in the active region exceed 1×10^{18} cm^{-3}, a population inversion occurs. In addition, when the current increases, the carrier density increases to; at some point, the transparency carrier's density and the optical gain become positive and greater than the internal loss. As a result, laser oscillation begins and the excess current above the threshold is converted into the intense laser output very efficiently [18]. Thus, for the laser design, it is important to have a positive gain at the intended laser wavelength. Fig. 2 shows the gain spectra, according to Eqs. (7) to (10), for different carrier densities and assuming that n=p (from $0.5 \times 10^{18}cm^{-3}$ to $0.5 \times 10^{19}cm^{-3}$). It is clear that the structures B and A operate at the wavelength range of 1.27-1.33µm because of MQW's positive gain. The maximum laser gain is about 3500 1/cm that is in good agreement with the numerical calculations of Yadav and Xia [19-21]. Fig. 3 presents the mode spectra of the proposed structures. As can be seen, the both structures B and A operate single mode at 1.325 µm. Therefore, our proposed material composition of the active region is suitable for operating the lasers in optical communication systems because of the output wavelengths of the two structures that lie within the appropriate wavelength range. Fig. 4 displays a transparency carrier density of about $1.5 \times 10^{18}cm^{-3}$ for the proposed MQW, which is in excellent agreement with Yi-Wei's study [22]. At this carrier density, the laser beam is produced, which is very close to the inversion population density. For the high performance of semiconductor lasers, MQW should be operated at the lowest possible transparency carrier density where MQW produces high positive gain since the gain saturates at high carrier densities.

Several factors must be considered when designing a semiconductor laser; they include bandgap, strain, and doping of all laser layers. The

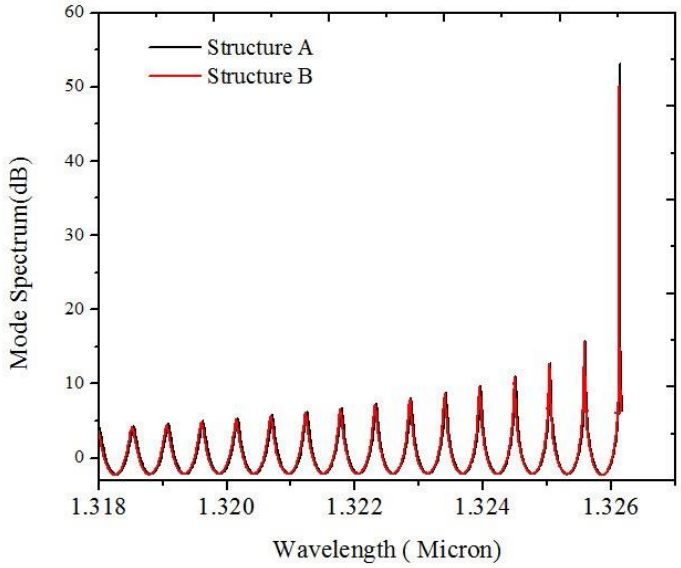

Fig. 3. Mode spectrums of structure B and structure A.

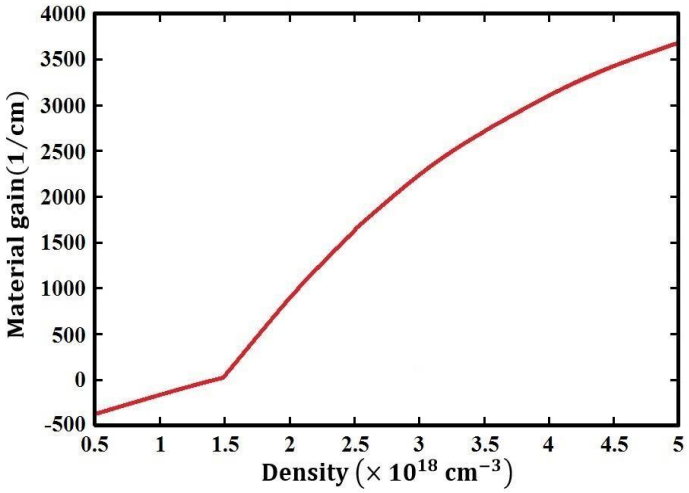

Fig. 4. Peak gain vs. carrier density.

most important point in laser operation is the carrier transport between quantum wells and SCL layers. Carrier leakage has been a critical issue since the invention of semiconductor lasers. The band offset of the active region and p-waveguide layer forms the barrier heights. Carriers with higher energy than barrier heights are able to escape the quantum wells. Electrons are able to escape more steadily due to higher mobility and diffusion constant in comparison to holes [15]. The vertical electron energy band diagrams of the structure B and the structure A at a current of 90 mA are indicated in Fig. 5 (a) and Fig. 5 (b), respectively. The importance of energy band diagrams for semiconductor lasers is attributed to the fact that many important physical and optical properties of the device can be explained using their energy bandgap. In structure B, because of the large bandgap of the cladding layers, the energy of electrons injected from the n-cladding layer is quite high. Electrons with high energy content must firstly diffuse and drift along the n-SCL into the edge of MQW and then be captured with a finite quantum mechanical probability into the

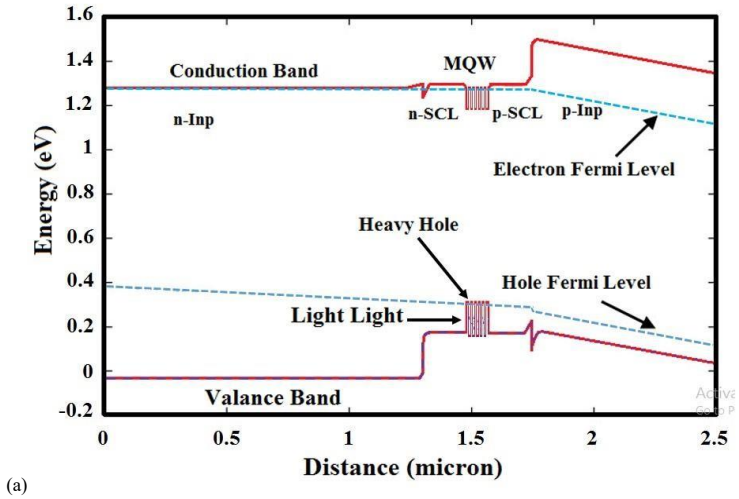

(a)

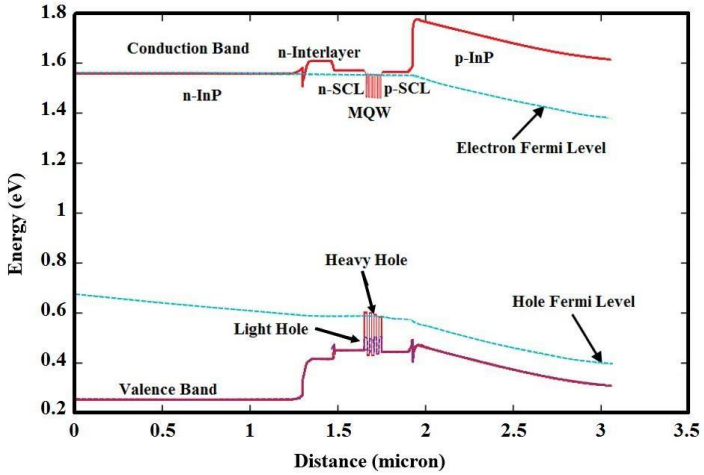

(b)

Fig. 5. Energy band diagrams of the (a) structure B and (b) structure A at 90 mA.

MQW. The quite high energies lead to the electron transport across the MQW into the opposite p-cladding layer, recombine with the holes existing over there, and form a severe leakage current [3]. In structure A, the n-interlayer bandgap energy is higher than the n-SCL layer bandgap energy, suggesting that the energy of electrons in structure B is higher than in structure A in the n-side region. In comparison, in structure A, a higher bandgap difference (i.e., 0.05 eV) exists between the p-SCL and p-cladding layer compared with structure B. Therefore, the electrons meet higher barrier on their way to the p-cladding layer, leading to a reduced number of the electrons that can run away from the active region of structure A. Thus, the electron leakage current must be reduced.

The band energy diagram of asymmetric laser structure is similar to that achieved by Qing [12, 13]. This means that our proposed structure also eliminates the barriers to vertical hole transport, while incurring a minimum penalty to electron leakage from the active region.

Fig. 6 confirms the idea of reduced electron leakage. The vertical electron current density profiles of the two structures at 90 mA are illustrated in Fig. 6. Ideally, the electrons and holes meet each other in the quantum wells and must recombine completely; however, some electrons leave the quantum wells and leak into the SCL. Based on Fig. 6, the electron injection current density of the two structures is equal but decreases in the multi-quantum wells. When the electrons are injected from the n-side layers into

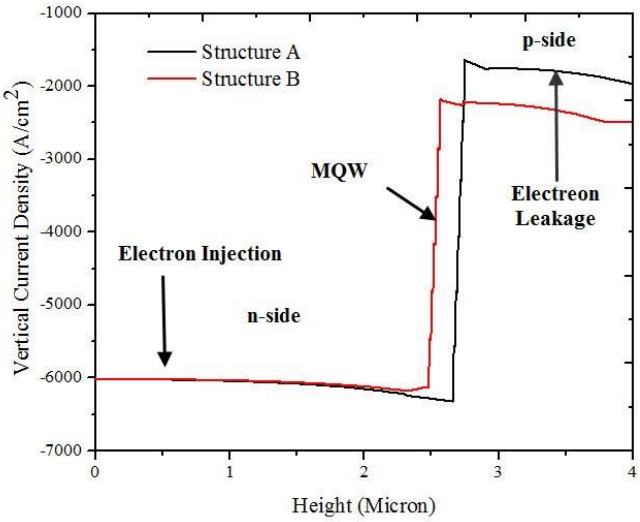

Fig. 6. Electron current densities of structure B and structure A at 90 mA.

the MQWs, they recombine with the holes over there; thus the electron current density reduces in the quantum wells [23]. It is obvious that the electron current density reduction of structure A is larger than that of structure B in the quantum wells, suggesting that more electrons combine with the holes in MQWs in structure A than that of structure B. Outside the active region, structure A possesses a smaller electron leakage current density compared with structure B. Comparing the electron current density to Qing's results confirms that our proposed structure also effectively reduces the leakage current, which is comparable to recent investigations [13].

A decrease in the electron leakage current definitely affects the laser performance, which is discussed in the following. We consider the recombination processes in MQWs. Because the electron current density changes in the MQWs, it identically changes the carrier density and then the recombination rates. It is of significant scientific interest to understand the carrier recombination mechanism in semiconductor lasers. One of the most important laser parameters affected by recombination processes is the threshold current. Minimizing the threshold current maximizes the device's slope efficiency. Hence, it is vital to understand the carrier recombination changes with waveguide changes. Recombination mechanisms can, in general, be classified into two groups. Radiative recombination occurs when an electron in the conduction band recombines with a hole in the valence band and the excess energy is emitted in the form of a photon. The optical process associated with radiative transition is stimulated emission, in which the emitted photon has exactly the same energy and momentum as the incident photon; this forms the basis for laser production. The increase of stimulated recombination greatly affects the semiconductor laser's performance such as threshold current decreasing and slope efficiency increasing. Non-radiative recombination of an electron-hole pair is characterized by the absence of an emitted photon in the recombination process. The non-radiative recombination process that affects the performance of semiconductor lasers is called Auger recombination. This mechanism, which involves four particles states (three electrons and one hole), is important at high temperatures for semiconductor lasers [24]. In the design of semiconductor lasers, a high attention is paid to reducing Auger recombination. Fig. 7 (a) and Fig.7 (b) depict the recombination rates versus height in the active region of the two structures at 90 mA. As mentioned earlier, due to the more effective recombination of electrons and holes in the active region of structure A, the stimulated recombination of asymmetric waveguide laser diode increases in Fig. 7 (a). Increasing the stimulated recombination means that more electrons and holes are involved in photon generation; so, it is expected to reduce non-radiative recombination such as Auger recombination. Fig. 7 (b) exactly proves this claim. As seen, the Auger recombination rate decreases. Due to the large electron and hole concentrations

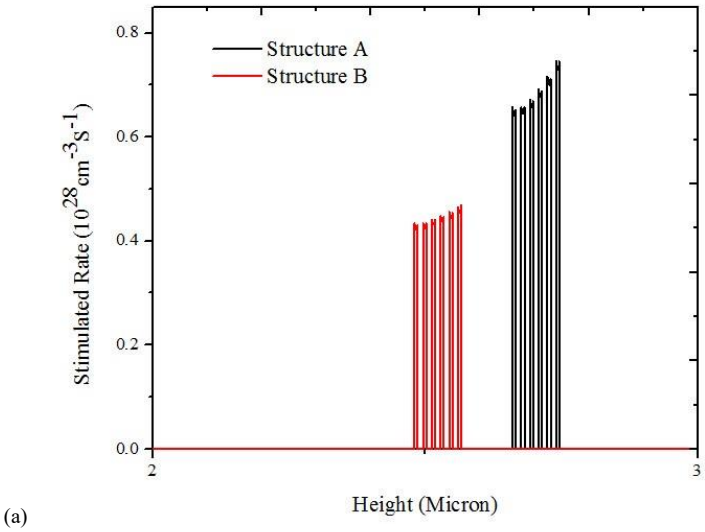

(a)

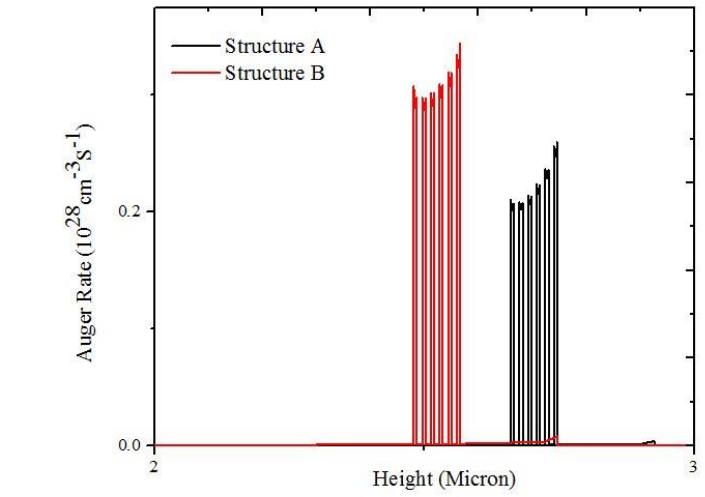

(b)

Fig. 7. (a) Stimulated recombination rates and (b) Auger recombination rates of structure B and structure A at 90 mA.

of the first and last quantum wells in the two devices, the stimulated and Auger recombination rates are non-uniform in the active regions.

At the second step, we notice the absorption change with a change in the waveguide structure. The MQW absorption is determined by free carrier absorption, which is estimated by the electron and hole concentrations in the quantum wells that do not contribute to photon generation. The absorption rates of structure B and A at 90 mA are compared in Fig. 8. A decrease in the absorption rate in an asymmetric waveguide laser can be seen this figure. An important result of increasing the stimulated recombination rate in structure A is the absorption reduction because a larger number of electrons and holes contribute to photon generation and thus free carrier concentration decreases. The increase in radiative recombination rate and the decrease in the non- radiative recombination rate and absorption confirm that the new structure with asymmetric waveguide enhances the efficient radiative recombination in device A; therefore, a better laser performance can be expected.

At the third step, we study the optical behavior of the two devices. Optical confinement is achieved due to the contrast of the refractive index between the narrow and wide bandgap materials

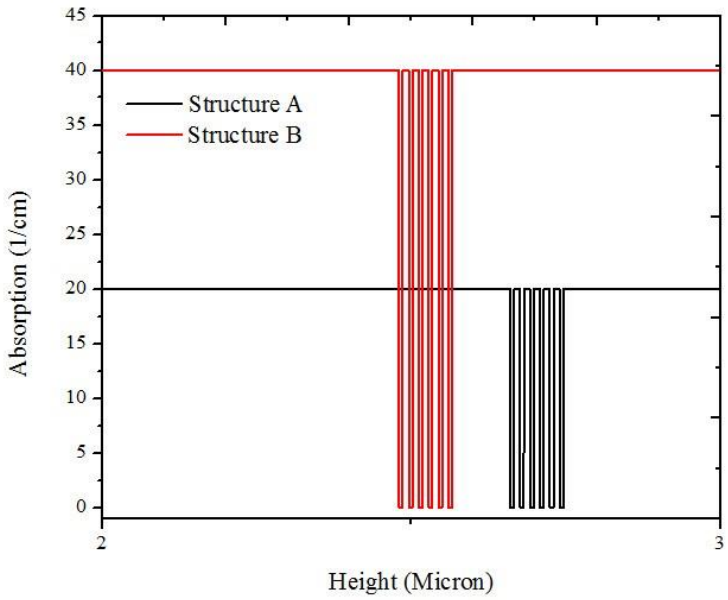

Fig. 8. Absorption rates of structure B and structure A at 90 mA.

used in the laser structure. This difference helps to confine the primary mode of light emitted by the laser to the gain medium. The modal gain of light propagating through the device is proportional to the overlap of the optical mode with the gain medium. Fig. 9 (a) and Fig. 9(b) illustrate the refractive index profiles and the resulting optical mode profiles and their overlap with central gain mediums in structure B and structure A, respectively.

The internal optical loss is defined as the loss of light from the lasing optical mode of the laser as it propagates down the waveguide structure. As shown in Fig. 9 (a) and Fig. 9 (b), the mode will be distributed across the multiple layers of the devices. P-type layers exhibit direct transitions through inter-valence band absorption (IVBA). Here, transitions do not require the assistance of phonon scattering, as they directly transit between the light hole, heavy hole and split-off bands. Due to the lack of dependence on phonon and impurity scattering processes, IVBA is thought to dominate contributions to optical mode loss in two diode lasers and optimize the waveguide design by minimizing this absorption. One method of reducing the impact of p-doped lasers, where the hole densities are significantly higher, is to minimize the overlap of the optical mode with these layers. Fig. 9 (b) confirms that our new asymmetric waveguide design satisfies both of these important issues. The overlap between the active region and the optical mode does not change significantly compared with the symmetric structure. On the other hand, the overlap of the optical wave with the p-doped layers decreases. Based on Fig. 9, it is clear that the wave intensity in structure A is higher than in structure B. Review of recent investigations on optical loss reduction in semiconductor lasers confirms that our proposed asymmetric waveguide reduces effectively the mentioned loss in comparison to other new waveguide structures [25].

Finally, we investigate the output power and voltage as the most important laser features. Fig. 10 (a) presents the continuous-wave light output power and voltage of structures B and A against the driving current by considering the thermal effects. As for the power-current, the output power, and threshold current are improved evidently, due to the suppression of electron leakage; this increases the stimulated recombination rate and decreases the Auger recombination rate in structure A. The results also show an improvement in the slope efficiency. The asymmetric waveguide's maximum output power is about 9 mW, which is comparable to the recent experimental findings of Khan and Arai [26, 27].

The current-voltage curve of laser diodes gives important information concerning the electrical characteristics of the device (Fig. 10 (b)). Below the

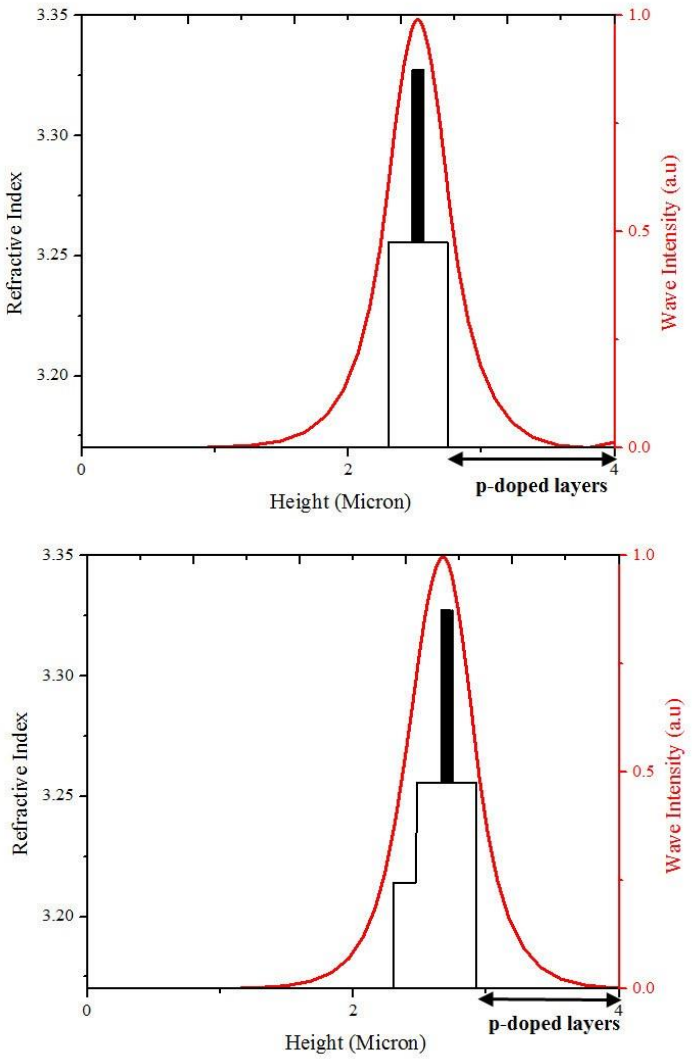

Fig. 9. Refractive index and optical mode profiles in (a) structure B (b) and structure A.

threshold, the I-V characteristic of the laser diode is that of a p-n junction with a series resistance. Above the threshold, the voltage across the laser diode saturates since the splitting of the quasi-Fermi levels is clamped because of the gain and the carrier density saturation [28]. Thus, the voltage across the laser diode under forward bias is the sum of the threshold voltage V_d and the voltage drops across the laser diode due to the series resistance (R_s):

$$V = V_d + IR_s. \quad (14)$$

where, V_d is defined as threshold voltage that is similar the turn on voltage for the diode lasing. The series resistance of diode lasers is one of their unique features because of its influence on the laser's maximum power. It also indicates quality of diode lasers and can be used as the production test. Semiconductor laser's series resistance is composed of semiconductor material resistance and resistance at the metal-semiconductor contacts of electrodes. Doping of the semiconductor layers and bandgap difference between the layers in the laser structure can also affect the laser's series resistance. This important parameter is determined by applying the linear fitting curve to the I-V characteristic plot above the threshold current. The slope of the fitting equation is series resistance [28]. Fig. 11 (a) and

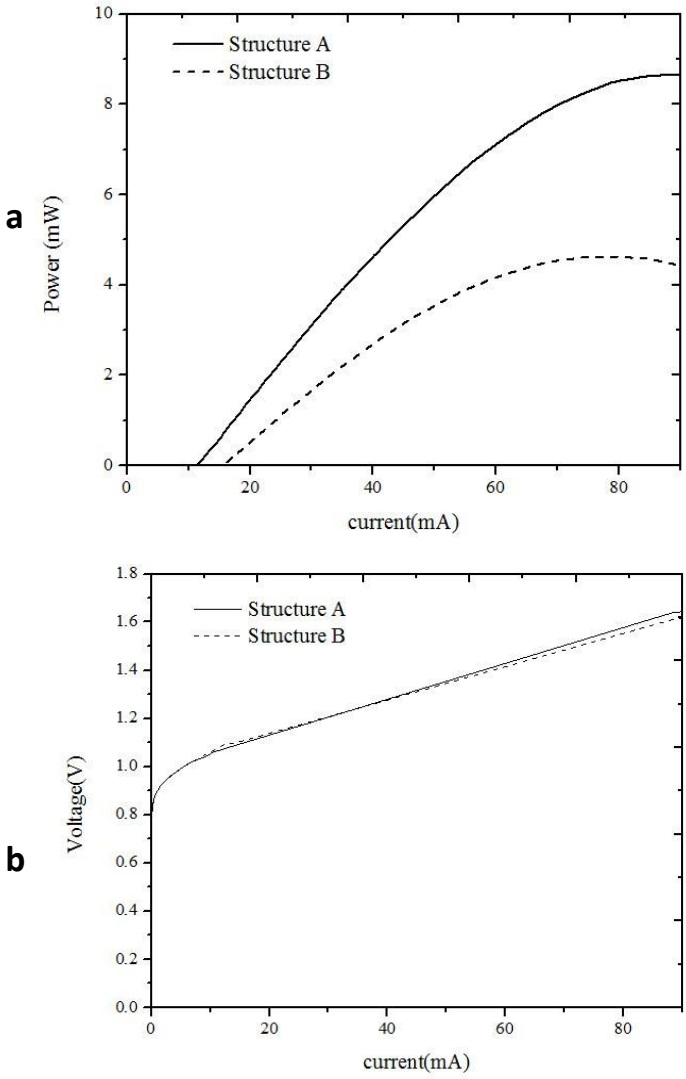

Fig. 10. (a) Continuous-wave optical light output power, (b) voltage vs. current.

Fig. 11 (b) show the I-V and the fitting curves of the two structures. Considering Equation 14, the slope of the fitting lines multiplied by 1000 indicates the series resistance of the laser diodes (In the horizontal axes of the Fig. 11 (a) and Fig. 11 (b) the unit of current is milliampere). So, the series resistance is 7 Ω and 6 Ω for structures A and B, respectively. As seen, the series resistance of the asymmetric structure is more than that of the symmetric structure. It can be explained by considering the changes in the laser bandgap and the carrier distribution by changing the device structure. In structure A, due to the increase of the bandgap height difference in the p-side of the device, an increase occurs in the hole concentration related to the p-cladding layer. By increasing the hole concentration and decreasing the carrier's mobility in the p-junction, the device's series resistance increases too, leading to a consequent increase in the device's voltage. The value of V_d is 0.983 V in structure A and 1.001 V in structure B; This means that the new proposed structure is able to decrease the threshold voltage.

CONCLUSION

In conclusion, an asymmetric waveguide structure was employed to be replaced by conventional symmetric waveguides. The performance characteristics of InGaAsP laser diodes with symmetric and asymmetric structures were

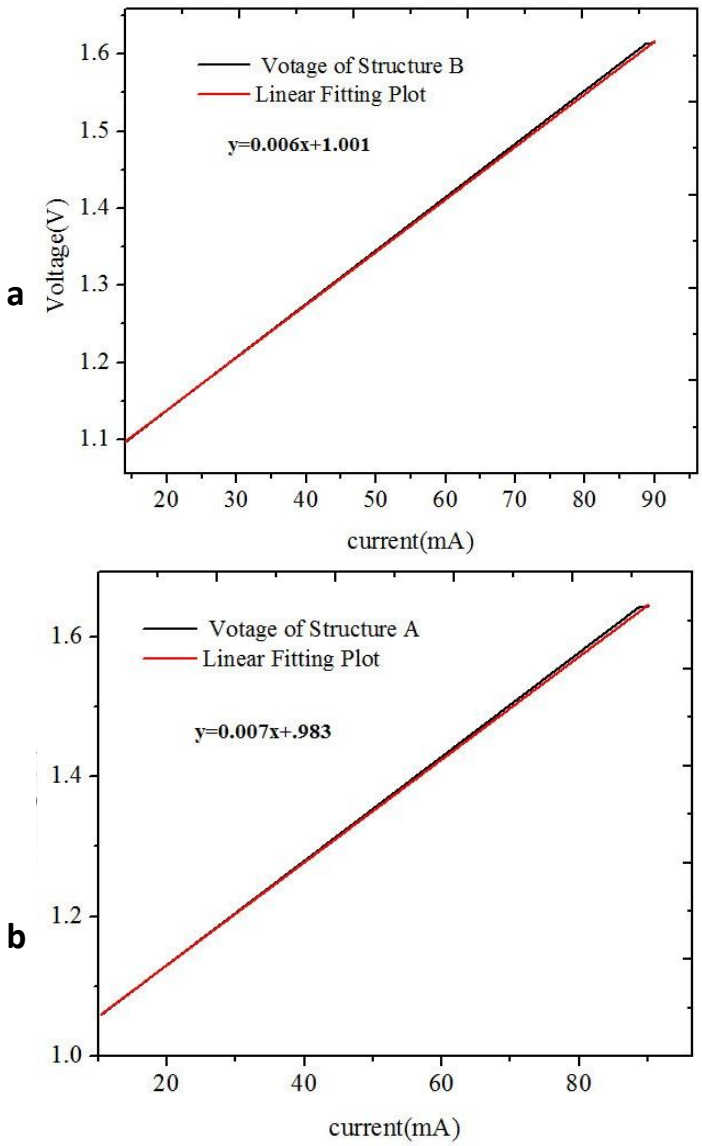

Fig. 11. V-I and fitting plots of (a) structure B, and (b) structure A.

numerically investigated using the PICS3D software. The results indicated that the asymmetric structure exhibits a higher output light power, slope efficiency, emission intensity, and series resistance, as well as a lower electron leakage and threshold current density under identical conditions, compared with the symmetric structure. The performances were greatly enhanced in the laser diode with asymmetric waveguide design because of the improved radiative stimulated recombination rate and declined non-radiative Auger recombination rate.

ACKNOWLEDGMENT

We express our sincere appreciation to the managers of Cross Light Inc. for providing us the advanced PICS3D simulation program (ver. 2008.12) and their kind support.

CONFLICT OF INTEREST

The authors declare that they have no competing interests.

REFERENCES

[1] Piprek J., (2019), On the reliability of pulse power

saturation models for broad area GaAsbased lasers. *Opt. Quant. Electron*. 51: 60-66.

[2] Abbasi S., Mahdieh M., (2019), Improvement of AlGaInAs/AlGaAs laser diode electro-optics characteristics by graded refractive index profile broadened waveguide. *Opt. Laser Technol*. 116: 155-159.

[3] Li X., Zhao D., Jiang D., Chen P., Liu Z., Zhu Ji., Shi M., Zhao D., Liu W., (2016), Suppression of electron leakage in 808 nm laser diodes with asymmetric waveguide layer. *J. Semicond*. 37: 014007-014011.

[4] Wu Y. F., J. C. Lee., (2017), Performance of nanostructures within InGaN-based multi-quantum-well light-emitting devices. *Appl. Sci*. 7: 380-387.

[5] Qiao Z., Tang X., Lee E., Lim P., Bo B. X., (2013), Large energy band-gap tuning of 980nm InGaAs/InGaAsP quantum well structure via quantum well intermixing. *Solid State Electron*. 79: 281-286.

[6] Zubov F. I., Maximov M. V., Shernyakov Yu. M., Kryzhanovskaya N. V., Semenova E. S., Yvind K., Asryan L. V., Zhukov A. E., (2015), Suppression of sublinearity of light–current curve in 850 nm quantum well laser with asymmetric barrier layers. *Electron. Lett.* 51: 1106-1111.

[7] Gordeev N. Y., Maximov M. V., Zhukov A. E., (2017), Transverse mode tailoring in diode lasers based on coupled large optical cavities. *Laser Phys.* 27: 086201-086207.

[8] Liu X., Zhao W., Xiong L., Liu H., (2015), Packaging of high power semiconductor laser. *Springer.* ISBN 978-1-4614-9263-4.

[9] Kwak J., Park J., Park J., Baek K., Choi A., T. Kim., (2019), 940-nm 350-mW transverse single-mode laser diode with AlGaAs/InGaAs GRIN-SCH and asymmetric structure. *Curr. Opt. Photonics*. 3: 583-589.

[10] Caggiano A., Marzano A., Teti R., (2016), Enhancement of a turbine vane manufacturing cell through digital simulation-based design. *Energies*. 9: 790-798.

[11] Huanga J., Evansa G., Butlera J., Jiangb L., Youngb P., Phanb D., Smithc D., (2017), Broadened waveguide laser structures at 780 nm. *Proc. SPIE.* 10086: 100860.

[12] Qing K., Shao-Yang T., Dan L., Rui-Kang Z., Wei W., Chen J., (2015), Optimization of high power 1.55-m single lateral mode fabry–perot ridge waveguide lasers. *Chin. Phys. Lett*. 32: 064203-064208.

[13] Qing K., Shaoyang T., Songtao L., Dan L., Ruikang Z., Wei W., Chen J., (2015), Fabrication and optimization of 1.55-m InGaAsP/InP high-power semiconductor diode laser. *J. Semicond.* 36: 094010-094016.

[14] Shen C. C., Hsu T. C., Yeh Y. W., Kang C. Y., Lu Y. T., Lin H. W., Tseng H. Y., Chen Y. T., Chen C. Y., Lin C. C., Wu C. H., Lee P. T., Sheng Y., Chiu C. H., Kuo H. C., (2019), Design, modeling, and fabrication of high-speed VCSEL with data rate up to 50 Gb/s. *Nanoscale Res. Lett.* 14: 276-282.

[15] Danesh Kaftroudi Z., (2019), Improving blue InGaN laser diodes performance with waveguide structure engineering. *J. Optoelec. Nanostruc.* 4: 1-8.

[16] Hisham H. K., (2018), Fiber optic telecommunication, fundamentals of photonics. *Am. J. Remote Sensing.* 6: 239-246.

[17] Zhang J., Nan J., Du W., Chu Y., Luo H., (2016), Dynamic analysis for a fractional-order autonomous chaotic system. *Discrete Dyn. Nat.* Soc. Article ID 8712496 | 13 pages.

[18] Ahmed W. W., Kumar S., Medina J., Botey M., Herrero R., Staliunas K., (2018), Stabilization of broad-area for semiconductor laser sources by simultaneous index and pump modulations. *Opt. Lett.* 43: 2511-2518.

[19] Xia M., Ghafouri-Shiraz H., (2015), A new optical gain model for quantum wells based on quantum well transmission line modeling method. *IEEE J. Quantum Electron*. 51: Article Sequence Number: 2500108.

[20] Yadav R., Lal P., Rahman F., Dalela S., Alvi P. A., (2014), Investigation of material gain of $In_{0.90}Ga_{0.10}As_{0.59}P_{0.41}$/InP lasing nano-heterostructure. *Int. J. Mod. Phys. B*. 28: 1450068.

[21] Yadav R., Lal P., Rahman F., Dalela S., Alvi P. A., (2014), Well width effects on material gain and lasing wavelength in InGaAsP/InP nano heterostructure. *J. Optoelectro. Engin.* 2: 1-6.

[22] Yi-Wei M., Yao W., Yang-Hua C., Zheng-Qun X., Qi L., Yan-Min D., Hui S., (2012), Characteristic optimization of 1.3 μm high-speed MQW InGaAsP-AlGaInAs lasers. *Chin. Phys. Lett*. 29: 064204-064209.

[23] Cai X., Li S., Kang J., (2016), Improved characteristics of ultraviolet AlGaN multiple-quantum-well laser diodes with step-graded quantum barriers close to waveguide layers. *Superlattice. Microst.* 97: 1-7.

[24] Underwood J. K., Briggs A. F., Sifferman S. D., Bank S. R., Gopinath J. T., (2018), Auger recombination in mid-infrared active regions. *CLEO: Appl. Technol.* Paper JTh2A.85.

[25] Edward Rees P., (2017), Characterisation of the waveguide dependence of optical mode loss in semiconductor lasers, cardiff university school of physics and astronomy. ISNI: 0000 0004 6496 305X.

[26] Khan M. Z. M., Alhashim H. H., Ng T. K., Ooi B. S., (2015), High-power and high-efficiency 1.3μm superluminescent diode with flat-top and ultra wide emission bandwidth. *IEEE Photon. J.* 7: 1600308.

[27] Arai M., Kobayashi W., Kohtoku M., (2013), *1*.3 μm range metamorphic InGaAs laser with high characteristic temperature for low power consumption operation. *IEEE J. Sel. Top. Quantum Electron*. 19: 1502207.

[28] Cataldo E., Lieto A. D., Maccarrone F., Paffuti G.,(2016), Measurements and analysis of current–voltage characteristic of a p-n diode for an undergraduate physics laboratory. *Cornel University.* arXiv:1608.05638.